ELSEVIER

Spectral analysis of boundary-layer transition on a heated flat plate

Ting Wang and Dadong Zhou
Department of Mechanical Engineering, Clemson University, Clemson, SC, USA

A spectral analysis was made for a boundary layer undergoing laminar–turbulent transition over a heated flat plate with free-stream turbulence intensities of 0.5% and 6.4%. Detailed boundary-layer measurements were made with a three-wire probe that simultaneously measured two velocity components and the temperature. The power spectra of u', v', and t', as well as their co-spectra, were analyzed. The spectral analogy and the differences between the momentum and thermal transports were investigated. The results showed that the location of maximum turbulence production ($y/d \approx 0.1$) coincided with the peak location of u'; whereas, the region of high turbulent shear ($y/d \approx 0.35$) produced little turbulence energy. The power spectrum of t' was mostly correlated with u' in the early to middle transitional flow, but it was significantly correlated with v' in the late transitional and early turbulent flow regions. The dissipation power spectra for both u' and v' evolved faster than their turbulence power spectra. $\overline{vt}$ seems to be transported by smaller eddies than $\overline{ut}$. A hypothetical energy transfer process during laminar–turbulent transition was then proposed.

Keywords: turbulent transition; spectral analysis; heat transfer; boundary layer

Introduction

One of the key features in boundary-layer transition from laminar to turbulent flow is the intermittent behavior (Emmons 1951). The characteristics of nonturbulent and turbulent regions are obviously different. The intermittency theory, proposed by Emmons and Narasimha (1958), considered the nonturbulent part and the turbulent part of the transitional flow as laminar flow and fully turbulent flow, respectively. However, some recent, conditionally sampled results (e.g., Kuan and Wang, 1989, 1990; Kim et al. 1994) have indicated that the nonturbulent part is highly disturbed and is different from conventional laminar flow and that the turbulent part is still evolving and is different from fully turbulent flow. These results were based on conditionally sampled profiles of the mean velocity, the Reynolds normal stresses, and the Reynolds shear stresses. To improve understanding of the fundamental mechanisms involved in the transitional boundary layer, it is believed necessary to obtain detailed spectral information. The present study was, therefore, undertaken to perform the spectral analysis for both flow and thermal structures in transitional boundary layers.

Boundary-layer spectral measurements rarely have been reported for boundary layers undergoing transition from laminar to turbulent flow. Suder et al. (1988) measured the streamwise velocity component fluctuation spectra in a boundary layer with a zero-pressure gradient at the point where the rms of the fluctuating velocities was a maximum. The boundary-layer spectra for the lowest free-stream turbulence intensity (0.3%) indicated amplification of the Tollmien–Schlichting (T–S) waves, which followed the behavior predicted by linear stability theory up to the point of turbulent bursting. The boundary-layer spectra for the 0.65% free-stream turbulence intensity case partially followed the behavior predicted by linear stability theory; however, the higher frequency fluctuations were not damped but rather were amplified as the streamwise distance increased until the turbulent bursting point was reached. When the free-stream turbulence intensity was elevated to 0.85%, the boundary-layer spectra showed the same trend as for the 0.65% free-stream turbulence intensity case, but they had a higher energy content at higher frequencies. As turbulent bursting was initiated, the energy of the spectra for all three cases increased at all frequencies. With the increase in the intermittency along the streamwise distance, the energy level increased over the whole frequency range, but the amplitude of the low-frequency disturbances diminished beyond a certain intermittency level. The energy level asymptotically reached a constant value as the boundary layer became fully turbulent. Similar results were reported by Sohn and Reshotko (1991).

Blair (1992) measured the streamwise velocity fluctuation spectra in the transitional boundary layer with a mild favorable pressure gradient ($K = 0.2 \times 10^{-6}$) and a 0.8% free-stream turbulence level. Prior to turbulent bursting, the spectra showed that the signal was dominated by lower frequency disturbances, while the high-frequency portion of the free-stream disturbance spectrum had been largely damped out. In the transition region, the conditionally sampled spectral distributions of the turbulent part, the nonturbulent part, and the total fluctuations were presented.

Address reprint requests to Prof. T. Wang, Department of Mechanical Engineering, Clemson University, Box 340921, Clemson, SC 29634-0921.

Received 26 May 1995; accepted 19 September 1995

Int. J. Heat and Fluid Flow 17: 12–21, 1996

655 Avenue of the Americas, New York, NY 10010

0142-727X/96/$15.00
SSDI 0142-727X(95)00082-8

Comparison of the spectral distributions for the turbulent part showed that the ratio of high-frequency to low-frequency power increased with the streamwise distance. Blair's results indicated that the ratio of production to dissipation was relatively high for early transitional turbulent bursts. To the authors' knowledge, other than the spectra of turbulence energy transport, the turbulent thermal energy spectra for a transitional boundary layer are still lacking in the literature.

The present experiments were conducted in a two-dimensional (2-D) wind tunnel with two free-stream turbulence levels at about 0.5% and 6.4%, respectively, on a heated flat plate. The study focused on three aspects: (1) examining the spectral distribution of fluctuations near the onset of spot formation; (2) examining the evolution of the spectral distribution of fluctuations in the transition process; and (3) examining the spectral analogy between the velocity fluctuation and the temperature fluctuation in the transition process.

Experimental program

Wind tunnel

The present research employed a 2-D, open circuit, blowing-type wind tunnel. A detailed description of the design considerations and construction specifications was documented by Kuan (1987). Air is drawn through a filter box and then forced through two grids, a honeycomb, a heat exchanger, a screen pack, and a 9:1 contraction nozzle before entering the test section. The flow rate can be adjusted steplessly by a constant-torque, variable-frequency motor controller. A suction fan and a low-pressure plenum were installed to provide boundary-layer suction at the leading edge.

Test section

The rectangular test section was 0.15 m wide, 2.4 m long, and 0.92 m high with an aspect ratio of 6. The large aspect ratio ensured two-dimensionality. One of the vertical walls of the test section was instrumented as the test wall. The test wall was composite, consisting of a custom-made, electric heater patch and 185 embedded thermocouples. Measurements were performed by traversing the probe through holes drilled on the wall opposite the test wall. The first measuring hole was located 20 cm downstream of the leading edge, and the rest were arranged so that they were 15 cm apart from each other. Detailed information on the heated test wall is documented in Wang et al. (1992) and Zhou (1993).

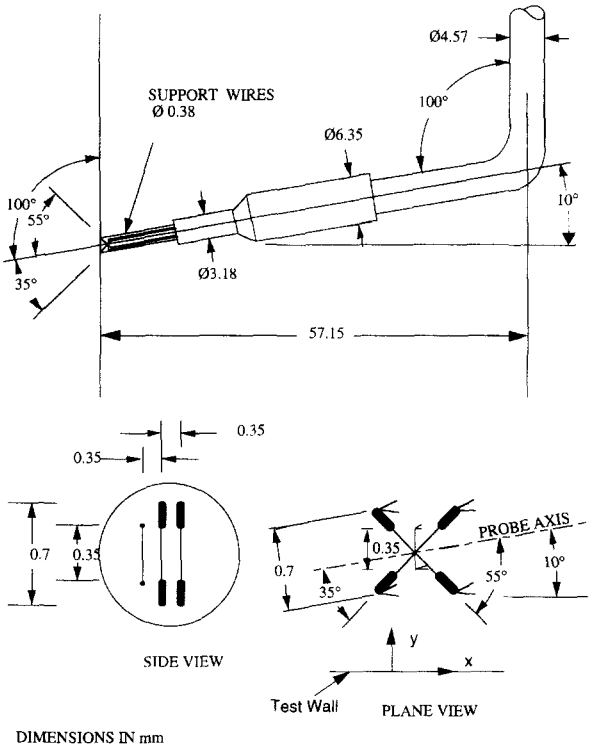

Figure 1 Three-wire boundary-layer sensor for measuring Reynolds stresses and heat fluxes

Instrumentation and measurements

A three-wire sensor, as shown in Figure 1, was especially designed to measure the instantaneous longitudinal velocity, the cross-stream velocity and the temperature simultaneously. Basically, and "X" array of 1.0-mm long, 2.5-μm diameter, gold-plated tungsten wires was used for velocity measurement. The sensing length was 0.5 mm, etched in the center. The spacing between the wires of the "X" array was 0.35 mm. The temperature sensor was a 1.2-μm, unplated platinum wire located 0.35 mm away from and in a plane parallel to the plane of the "X" array. To allow near-wall measurement and to reduce probe interference, the probe support was bent at an angle of 10° from the wire axis. However, the wires of the "X" array were still

Notation

$E_u(k)$, $E_v(k)$, $E_t(k)$	1-D spectra of u, v, and t
FSTI	free-stream turbulence intensity, $\sqrt{(u^2+v^2+w^2)/3}/\bar{U}_\infty$
k	wave number, m^{-1}
$P_{uv}(k)$, $P_{ut}(k)$, $P_{vt}(k)$	co-spectra among u, v, and t
t	instantaneous temperature fluctuation or time
T^+	mean temperature in wall units, $(\bar{T}_w - \bar{T})\rho c_p u^*/q''_w$
u, v	instantaneous streamwise and cross-stream velocity fluctuations
u', v', t'	rms values of u, v, and t
u^*	friction velocity $\equiv \sqrt{\tau_w/\rho}$
U^+	mean streamwise velocity in wall units, U/u^*
x	streamwise distance from the leading edge
y	distance away from the wall
Y^+	yu^*/ν

Greek

τ_w	wall shear stress
Γ	intermittency
Λ	integral length scale, $\bar{U}\int_0^\infty \overline{u(t)u(t+\tau)}/)/u^2 d\tau$
ρ	density

Subscripts

∞	in the free stream
w	at the wall

perpendicular to each other. A more detailed probe description and the qualification of this probe are contained in Shome (1991).

A TSI IFA 100 Intelligent Flow Analyzer System was used to operate the "X" array hot wires in a constant temperature mode to measure velocities. A DISA M20 temperature bridge was used to operate the cold wire in the constant current mode to measure temperature. A TSI Model 157 signal conditioner was used for low-pass filtering of the cold wire anemometer signals. The streamwise velocity, the cross-stream velocity, and the temperature were measured simultaneously by the three-wire probe.

The sampling rate was 2 kHz. A low-pass filter of 1 kHz was employed to remove aliasing errors. The choice of a 2 kHz sampling rate was a compromise between the existing data acquisition storage memory size, the frequency response of the cold wire (approximately 3000 Hz), the duration of each experiment (approximately 30 hours), and the significance of the information that can be obtained at frequency ranges higher than 1000 Hz. The three-wire probe simultaneously takes signals from two hot wires and one cold wire; because the cold wire had the poorest frequency response of the three, the sampling rate was primarily limited by the frequency response of the cold wire. To investigate the significance of spectra information beyond 1000 Hz, a higher sampling rate of 30 kHz was used for velocity signals in several locations in the transitional region. It was found that the energy beyond 1000 Hz was less than 1% in the near-wall region, less than 5% in the outer boundary layer, and approximately 10% in the free stream at a free-stream velocity of 12 m/s. The evolution of the spectra at the higher frequency end does not provide any further insight into the physics beyond the data taken at 2 kHz. Therefore, it is believed that the present data are adequate to indicate the trend of spectral evolution in transitional boundary layers and that the sampling rate is an optimum choice under the existing conditions. No compensation was made for the cold wire, because the frequency response (approximately 3000 Hz) of the cold wire is higher than the sampling rate (2000 Hz). Detailed information of the method for determining the frequency response of the cold wire can be found in Keller (1993).

Free-stream turbulence

Two free-stream turbulence levels were performed for this study. The lower-level case, with FSTI = 0.5% and $\overline{U}_\infty = 12.24$ m/s, was used as the baseline case. For the higher-level case, FSTI = 6.4% and $\overline{U}_\infty = 1.7$ m/s. The elevated turbulence was generated by a biplane grid inserted upstream of the wind tunnel contraction. The free-stream turbulence distribution, the integral length scale in the streamwise direction, and the power spectrum are shown in Figure 2. A detailed discussion of the integral length scale and the free-stream power spectra is contained in Zhou and Wang (1995). The method of Chua and Antonia (1990) was used for correcting temperature contamination of the hot wires.

The power spectrum of a fluctuation signal was taken as the square of the magnitude of the Fourier transform of the signal. The co-spectra of two fluctuations were taken as the real part of the multiplication of the Fourier transform of one signal and the conjugate of the Fourier transform of another signal. The fast Fourier transform (FFT) technique was used in the process. Each signal contained 1024 points, and each power spectrum was an average of 40 signals.

Results and discussion

In this experiment, a boundary layer was allowed to undergo transition naturally from laminar to fully turbulent flow. The results of the baseline mean velocity profiles and the mean temperature profiles, plotted in wall units, are shown in Figures 3

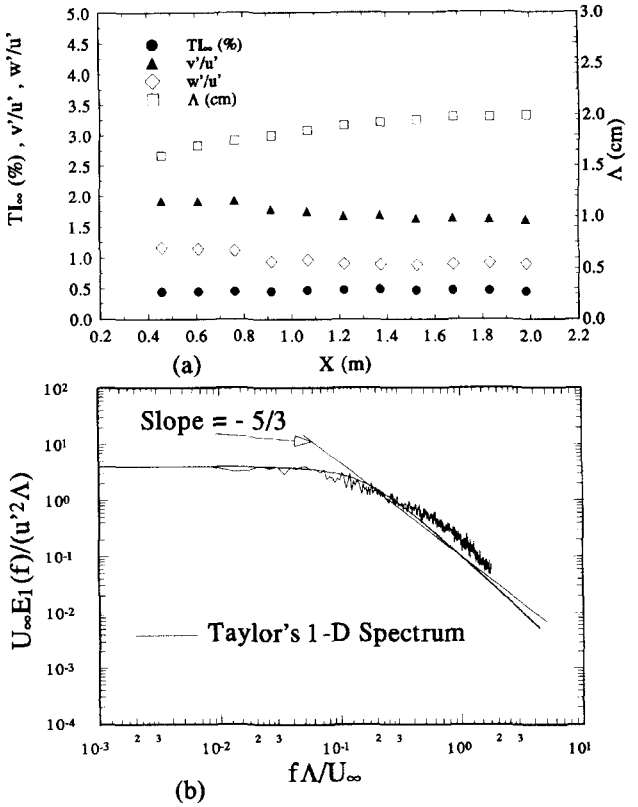

Figure 2 Free-stream turbulence (a) intensities and length scales and (b) spectral distribution

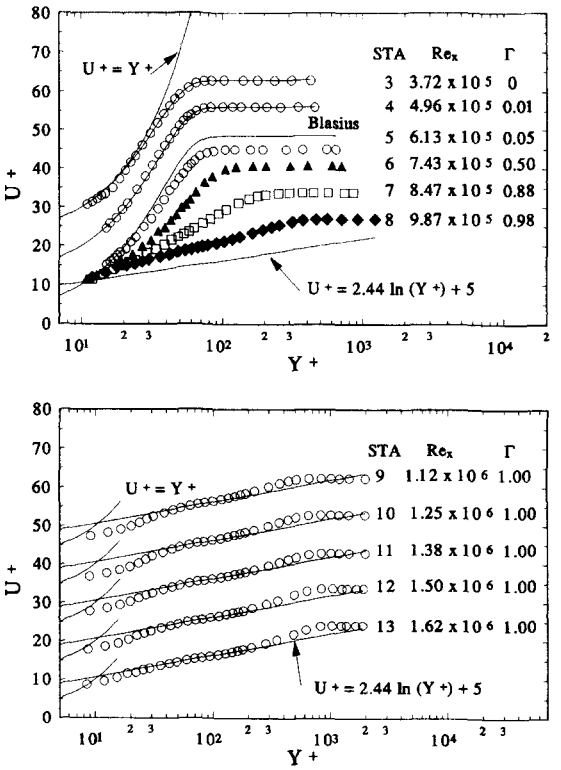

Figure 3 Mean velocity profiles, U^+ *versus* Y^+ for the baseline case

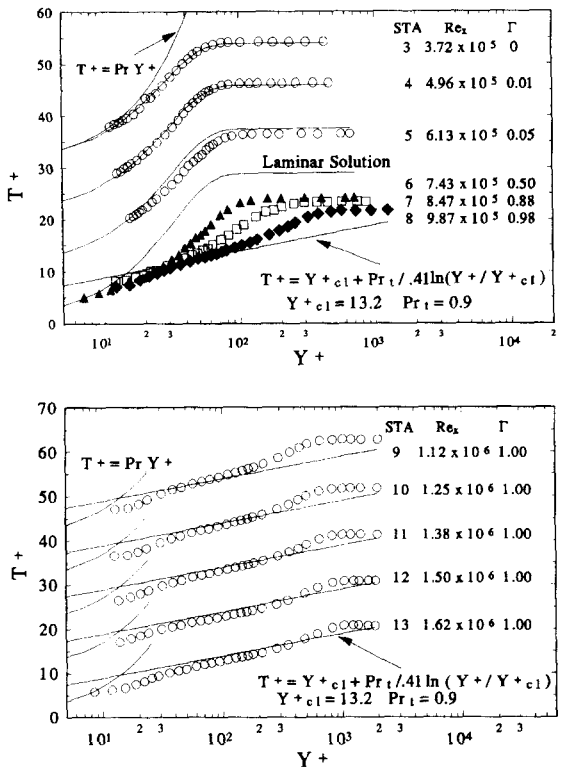

Figure 4 Mean temperature profiles, T^+ *versus* Y^+ for the baseline case

and 4, respectively. As seen in these two figures, the flow at stations 3 and 4, which follows the Blasius velocity distribution and has negligible intermittency, was clearly laminar flow. The flow at stations 9–13, which exhibited "law of the wall" characteristics over a sufficient range of Y^+ and had 100% intermittency, was clearly turbulent. The flow at stations 5–8, having intermittency between zero and one, was transitional, neither displaying turbulent, log-linear behavior nor matching the Blasius profile. The distributions of other statistical quantities across the boundary layer are documented in Wang et al. (1992, 1996).

Disturbances near the onset of transition

The transition started between stations 5 and 6. The baseline velocity signals at stations 3, 4, 5, and 6, taken at the location where u' reached its maximum across the boundary layer of each station, are shown in Figure 5. As shown in this figure, the velocity signals at stations 3 and 4 were dominated by low-frequency oscillations. At station 5, relatively higher frequency fluctuations appeared in the velocity signal. Such relatively higher frequency oscillations are manifestations of typical 2-D (T–S) instability waves; they are not turbulent fluctuations. At station 6, the flow was obviously intermittent between the region with sinusoidal-like, low-frequency fluctuations and the region with high-frequency fluctuations. According to the linear instability theory, the most amplified T–S wave frequency range at stations 3 to 6 for the baseline case is approximately between 40 Hz and 200 Hz, or between 60 m^{-1} and 250 m^{-1} in terms of wave numbers.

To see the amplified disturbances clearly, velocity signals that have been high-pass filtered to retain wave numbers above 60 m^{-1} were taken, and the results are shown in Figure 6. As shown, the T–S wave fluctuations were amplified between stations 4 and 5.

To see the velocity fluctuation energy distributions over different frequencies, one-dimensional power spectra of the longitudinal velocity fluctuations were processed from stations 3 to 6 at the maximum u' locations, as shown in Figure 7. As this figure illustrates, most of the fluctuation energy at stations 3 and 4 was contained in the very low wave number range (95% was under 60 m^{-1}). At station 5, the fluctuation in the T–S wave number range (60 ~ 250 m^{-1}) was amplified. At station 6, the fluctuation energy contained in the high wave number range was much higher than that at stations 3 to 5.

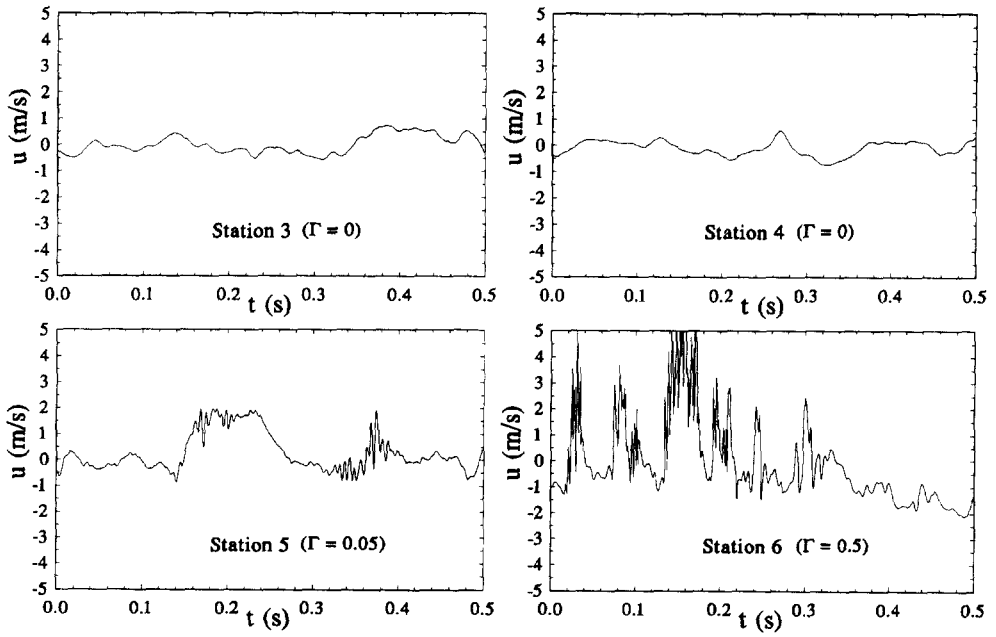

Figure 5 Velocity u signals, at maximum u' locations for the baseline case

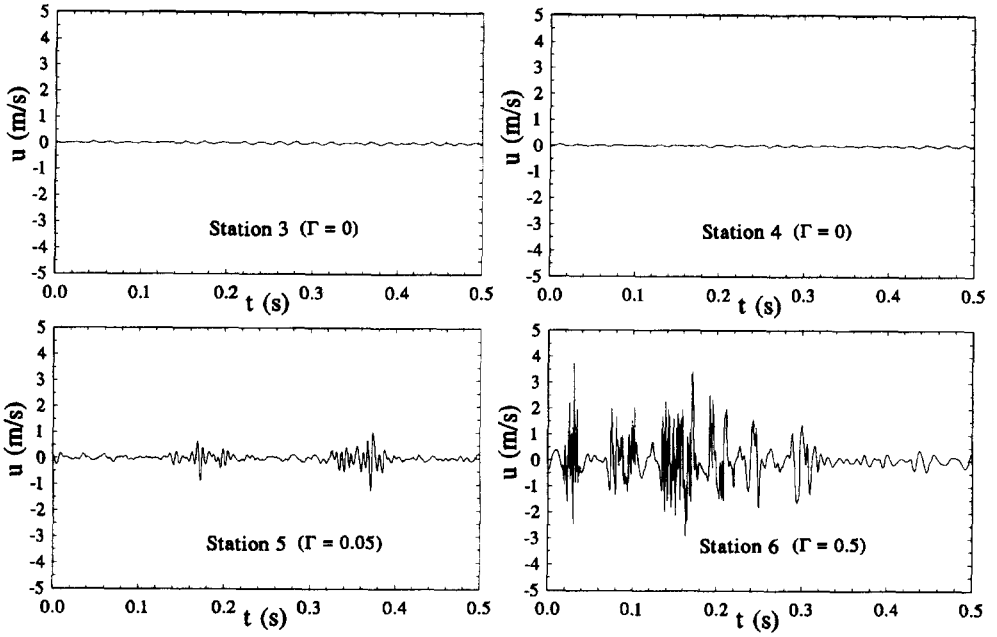

Figure 6 Velocity u signals high-pass filtered for $k > 60$ m^{-1} (or 40 Hz) at maximum u' locations for the baseline case

In Figure 7, some "humps" (sinusoidal-like waves) are apparent in the power spectrum at station 5. Generally, such "humps" in a spectrum can be caused by two possible influences: (1) the finite window effect on some sinusoidal fluctuations contained in the time-domain signal; or (2) nonperiodic wave forms, such as nonperiodic pulses, in the time-domain signal. To investigate the source of these humps, the power spectrum of each data piece was examined. An average power spectrum is an average of the power spectra for 40 datapieces; each datapiece contains 1024 datapoints obtained in a sampling duration of 0.512 seconds. These humps only appeared in some of the power spectra of those signals containing nonperiodic, finite-width impulses. One such impulse is shown in Figure 8. This impulse is clearly related to the change of the mean value as the signal passed a turbulent spot or wave packet. This impulse may be recognized as the first turbulent wave packet observed in the velocity signals. If this turbulent wave packets were removed, the humps in the power spectrum of the velocity signal would disappear, as shown in Figure 9. Therefore, a sinusoidal-like power spectrum signifies the earlier transition region that occurs when distinctive turbulent wave packets pass nonperiodically. These sinusoidal humps disappear when the occurrence of the turbulent wave packet; i.e., the intermittency, increases, as shown at station 6 in Figure 7. A region of high energy contained between 60 and 250 m^{-1} can be seen even after removal of the

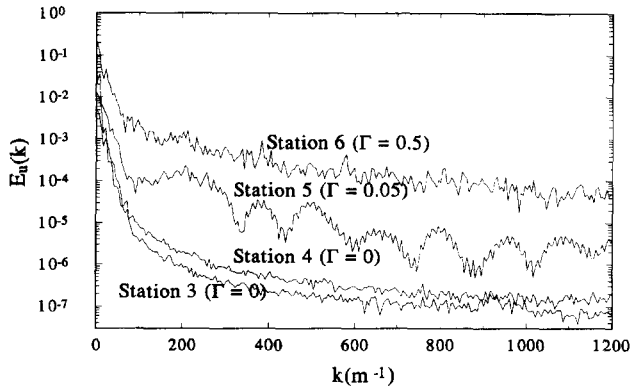

Figure 7 Power spectra of u velocity fluctuations at maximum u' locations for the baseline case

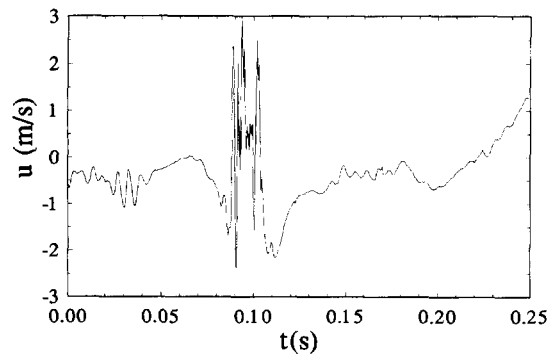

Figure 8 Velocity signal containing a turbulent wave packet at station 5 for the baseline case

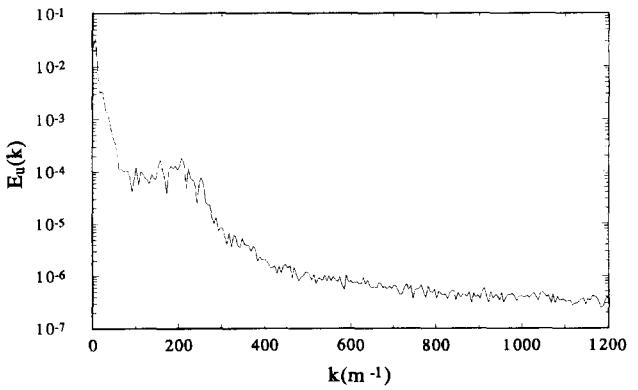

Figure 9 Power spectrum of the signal in Figure 7 after removal of the turbulent wave packet at station 5 for the baseline case

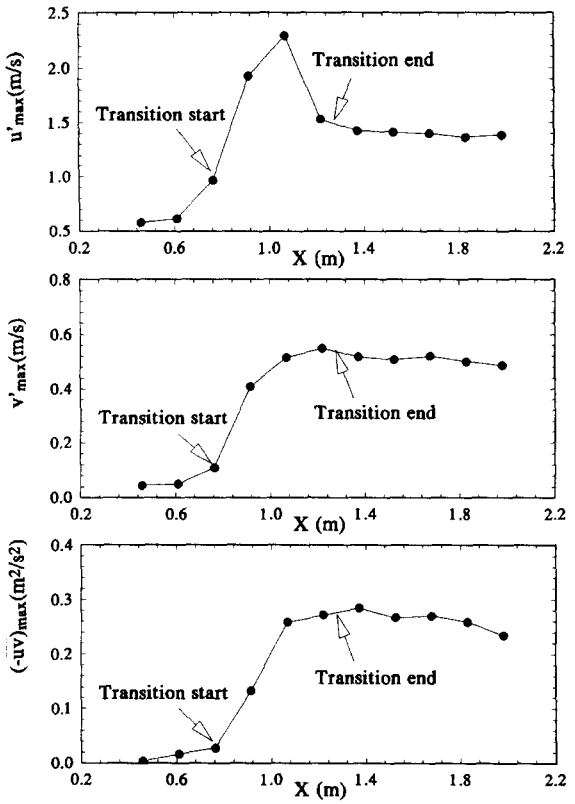

Figure 10 Streamwise evolution of peak velocity fluctuations and Reynolds shear stresses for the baseline case

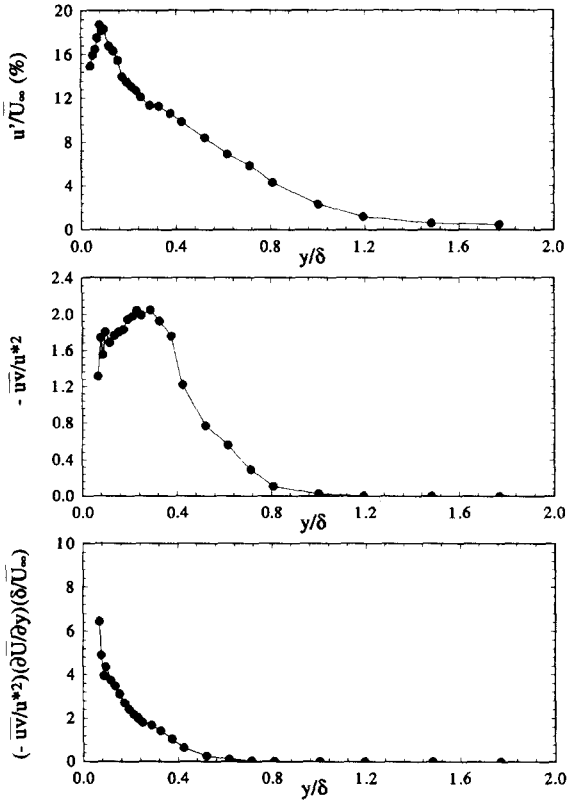

Figure 11 Distribution of Reynolds stresses and turbulent energy production at station 7 for the baseline case

wave packet in Figure 9. This verifies the statement made earlier that the linear T–S wave frequencies contribute to the oscillations of the nonturbulent part of the velocity signals between wave packets.

Spectral distributions of velocity fluctuations in wave packets and their streamwise evolution in the transition process

Before discussing the spectral distributions of the velocity fluctuations, it would be helpful to review the streamwise evolution of the peak u', v', and $\overline{uv}$ values during the transition process, as shown in Figure 10. Each point represents the maximum value across the boundary layer at a fixed x-location. As shown in this figure, the peak value of u' at each station reached its maximum value at approximately two-thirds of the transition region (station 7, $X = 1.07$ m; $\Gamma = 0.88$), and then decayed gradually to a nearly constant value in the turbulent region. However, the peak values of v' and $\overline{uv}$ increased to their maximum values in the later part of the transition region, and each maintained an approximately constant value into the turbulent region. Further discussion of possible energy transport related to these phenomena can be found in Kuan and Wang (1990) and is not repeated here.

The peak locations of u' and $\overline{uv}$ in the boundary layer at station 7 in the transition region, as replotted in Figure 11, were very different. The maximum u' occurred at around $y/\delta = 0.1$; whereas, the maximum $\overline{uv}$ (approximately twice the wall shear) occurred at around $y/\delta = 0.35$ (or $Y^+ \approx 70$). To our intuition, the region of high u' should have been an indication of high turbulent energy production. To check on this, the turbulence energy production term $\{-\overline{uv}\partial u/\partial y\}$, which extracts energy from the mean flow, was calculated and normalized, and the results are shown in Figure 11. The results indicate that the peak location of the local turbulence production coincided with the peak location of u'. This evidence implies that the high u' values are more likely caused by local turbulence production than by convection from upstream.

It is interesting to find out what causes the high Reynolds shear stress, $\overline{uv}$. Because the region of maximum $\overline{uv}$ values do not coincide with those of turbulent production, the comparison made in Figure 11 does not suggest that high Reynolds shear stress is related to high turbulence production. However, because the maximum $\overline{uv}$ occurred at around $Y^+ \approx 70$, it was conjectured that the region of high Reynolds shear stress may have been a manifestation of conventional vortex break-up activity or fluid ejection attributable to bursting. Physically, this conjecture combined with the results in Figure 11 suggests that the breakups that occurred at the tip of the hairpin vortices might have produced

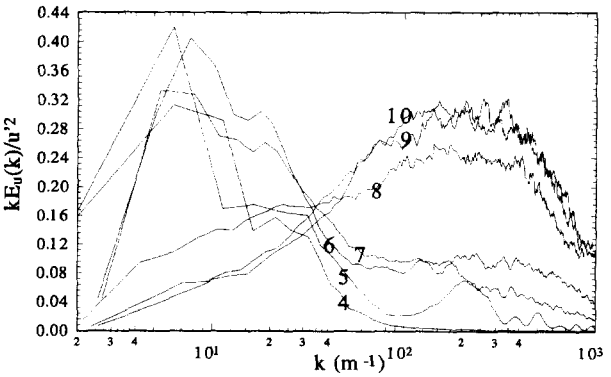

Figure 12 Power spectra of u velocity fluctuations at the maximum u' locations for the baseline case

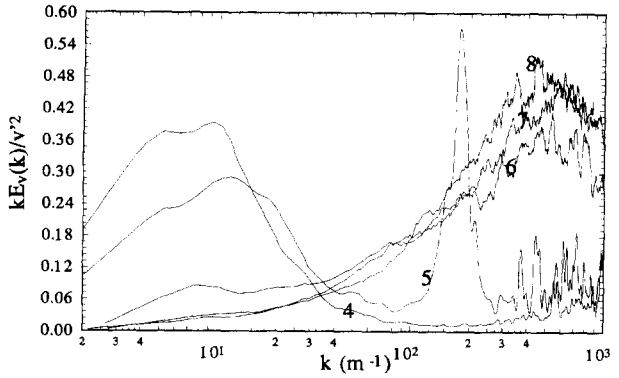

Figure 13 Power spectra of v velocity fluctuations at the maximum u' locations for the baseline case

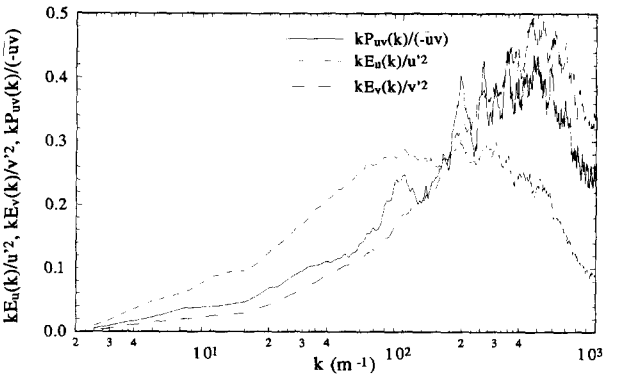

Figure 15 Comparison among $E_u(k)$, $E_v(k)$, and $P_{uv}(k)$ at the maximum u' location of station 12 for the baseline case

large turbulent shear stress, rather than turbulence energy, in a magnitude of twice the local wall shear.

Spectral analysis of the u and v velocity fluctuations can provide further information about the energy transfer process.

As discussed in the preceding section, once the transition was initiated near station 5, the power spectrum in the high wave number range increased rapidly with increasing distance downstream. This increase can be seen in Figure 12. The power spectrum at the wave number range higher than 60 m^{-1} is believed to be derived mainly from the fluctuations in the turbulent wave packets. Information on spectra with frequencies higher than 1000 Hz (or wave numbers higher than approximately 1000 m^{-1} for the baseline case) is not available, because the sampling rate was 2000 points/s, and the Nyquist principle implies that spectra information is only meaningful for frequencies lower than one-half of the sampling frequency.

One-dimensional power spectra of u and v and their co-spectra obtained at the maximum u' locations for the baseline case, normalized by the corresponding variance, are presented in Figures 12, 13, 14, and 15. In these figures, the power spectra or co-spectra are weighted with wave number in the form $kE(k)$ and are plotted as a function of $\ln(k)$. The area under the curve represents the total energy or variance, which equals 1 after normalization since

$$E(k)dk = kE(k)d\ln(k) \qquad (1)$$

Similar to the evolution of the spectra of u (Figure 12), the evolution of the spectra of v in Figure 13 also shows that the fraction of energy contained in the low wave number range ($k < 60$ m^{-1}) decreased while the fraction of energy contained in the high wave number range ($k > 60$ m^{-1}) increased during the transition process. The evolution of this process was faster for v than it was for u. For v, the power spectra changed dramatically from station 5 to station 6 and reached an equilibrium from station 7 to station 10. It is interesting to see that the instability at around 180 m^{-1} at station 5 is especially amplified in Figure 13. A rapid change in the u power spectra occurred later between station 7 and station 8, and equilibrium was not reached until downstream of station 9. These observations are consistent with the maximum u' and v' evolutions shown in Figure 10.

In the late transition and early turbulent regions (downstream of station 8), there was a plateau of high energy content between 100 m^{-1} and 400 m^{-1} for the power spectra of u (Figure 12). In contrast, the range of high wave number for the power spectra of v was within 300 m^{-1} to 1000 m^{-1}. The peak locations of the power spectra of v occurred near the end of the plateau region of the power spectra of u. This may imply that the energy transfer from the longitudinal velocity fluctuations (u) to the cross-stream velocity fluctuations (v) is most effective in the high wave number range (between 300 m^{-1} and 1000 m^{-1} for the baseline case). This is consistent with the cascading theory of turbulence energy, with the recipients of energy being in smaller eddies. This transfer of energy from u to v may largely take place through the correlation with the pressure fluctuations (return-to-isotropy terms), as is mentioned later in Figure 18. The pressure fluctuations seem to be the only communication channel between the u'^2 and the v'^2 transport equations.

The co-spectra between u and v at station 6 in the early transition region and at station 12 in the turbulent region are shown in Figures 14 and 15. In these figures, the co-spectra are seen to have been affected by both velocity fluctuations, but the effect of v is dominant. This suggests that the turbulent shear

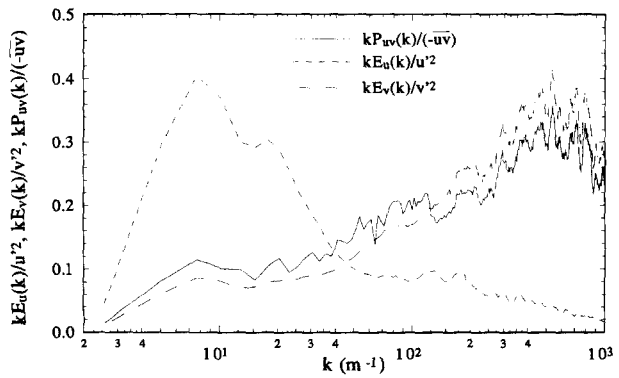

Figure 14 Comparison among $E_u(k)$, $E_v(k)$, and $P_{uv}(k)$ at the maximum u' location of station 6 for the baseline case

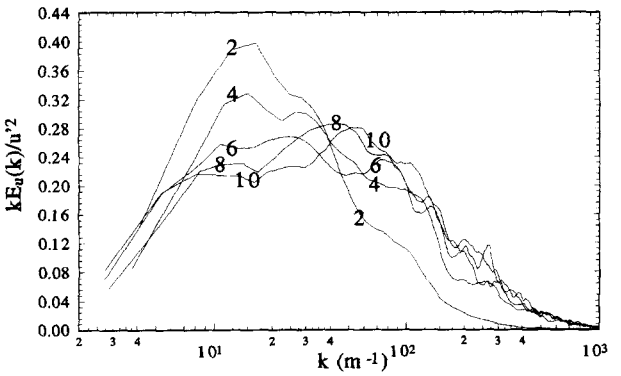

Figure 16 Power spectra of u velocity fluctuations at the maximum u' locations for the case with FSTI = 6.4%

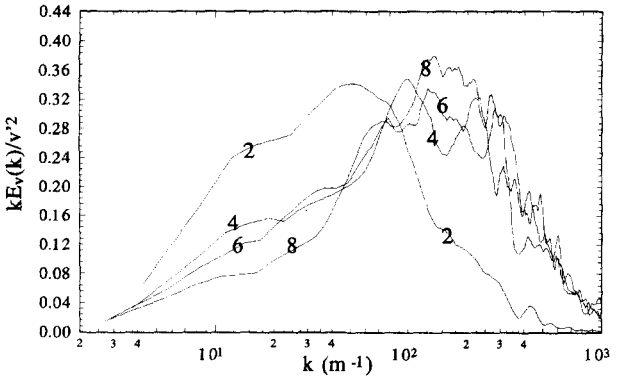

Figure 17 Power spectra of v velocity fluctuations at the maximum u' locations for the case with FSTI = 6.4%

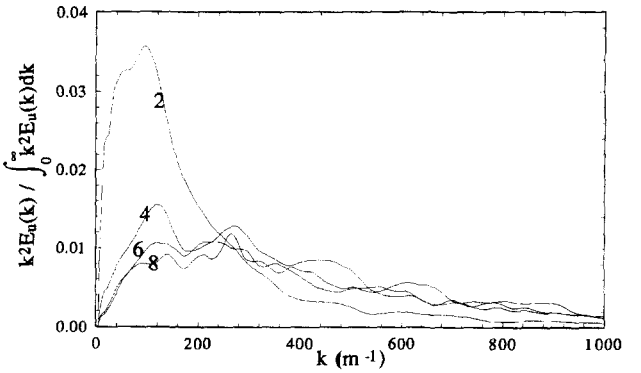

Figure 19 Normalized dissipation energy spectra of u'^2 at the maximum u' locations for the case with FSTI = 6.4%

stress is predominantly driven by v, even in the presence of higher magnitudes of u. This provides an important insight into the dominance of v activity in the transport of turbulent shear stress. The higher magnitudes of u' below 60 m^{-1} are streamwise unsteadiness, so it does not correlate well with the turbulent shear.

Elevated FSTI case

The normalized power spectra of the u and v velocity fluctuations for the elevated FSTI case (6.4%) at maximum u' locations are shown in Figures 16 and 17. In these figures, the turbulence energy is negligible beyond 1000 m^{-1}. For the fluctuations, the energy above 30 m^{-1} (Figure 16) was amplified; the energy below 30 m^{-1} was damped but maintained at a higher level than for the baseline case (Figure 12). The peak for the u spectrum in the late transitional and early turbulent region occurred at around 40 ~ 70 m^{-1} for the 6.4% FSTI case (Figure 16), while the peak occurred at around 200 ~ 400 m^{-1} for the baseline case (Figure 12). The peak of the v spectrum in the late transitional and early turbulent region took place at around 100 ~ 200 m^{-1} for the elevated FSTI case (Figure 17), while the peak is at around 500 m^{-1} for the baseline case (Figure 13). These differences in the wave number ranges containing the primary turbulence energy may have been caused by the difference between the free-stream velocities. Recall that the free-stream velocity was 12.24 m/s for the baseline case and 1.7 m/s for the high-turbulence case.

The term $\overline{(\partial u/\partial x)^2}$ of the dissipation energy terms

$$\left\{-2\mu\overline{\frac{\partial u}{\partial x_k}\frac{\partial u}{\partial x_k}}\right\}$$

in the u' transport equation (see Figure 18) can be estimated from the u spectrum. Based on Taylor's hypothesis, $\overline{(\partial u/\partial x)^2}$ can be shown to be proportional to

$$\frac{4\pi^2}{\overline{U}^2}\int_0^\infty k^2 E_u(k)\,dk$$

$\overline{(\partial u/\partial x)^2}$ is used here to approximately represent the dissipation energy terms in the u'^2 transport equation. Similarly, $\overline{(\partial v/\partial x)^2}$ is used to approximately represent the dissipation energy terms

$$\left\{-2\mu\overline{\frac{\partial v}{\partial x_k}\frac{\partial v}{\partial x_k}}\right\}$$

in the v'^2 transport equation. The streamwise evolution of the normalized spectral dissipation energy distributions of u' and v' for a low-velocity, high-free-stream turbulence case ($\overline{U}_\infty = 1.7$ m/s; FSTI = 6.4%) are shown in Figures 19 and 20. By comparing these two figures with the u and v spectra in Figures 16 and 17, it is apparent that the evolution of the spectral distribution of the dissipation energy was faster than that of the corresponding turbulence power spectrum. The evolution of the dissipation energy distributions for the u component was similar to that for the v component, with more energy being dissipated at a higher

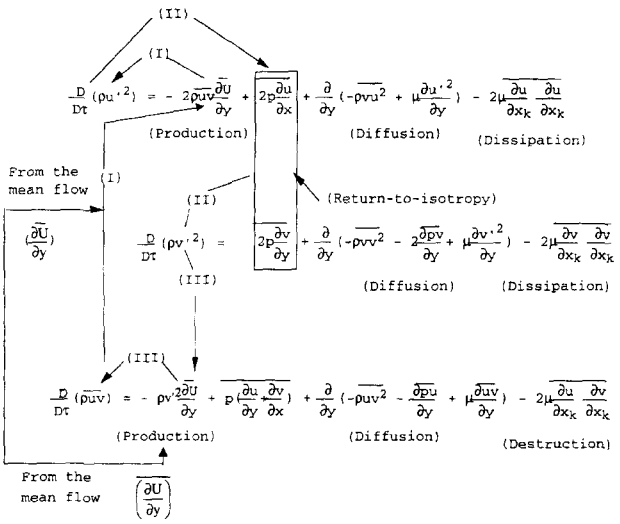

Figure 18 Hypothetical primary energy transfer processes in a transitional boundary layer

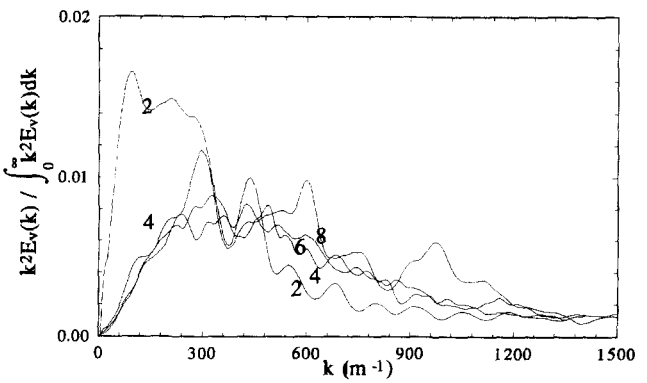

Figure 20 Normalized dissipation energy spectra of v'^2 at the maximum u' locations for the case with FSTI = 6.4%

wave number range as the transition proceeded. This implies that the cascading process at a high wave number (with small eddies) is faster than at a low wave number (with large eddies).

Based on the aforementioned discussion, the major energy transfer process in the transition region can be hypothesized, as in Figure 18. Once the bursts occur at the final stage of the formation of 3-D vortices, a turbulent shear stress distribution $(\overline{uv})$ forms around the bursts at about $Y^+ \approx 70 \sim 100$ (Figure 11), and energy transfers from the mean flow to the longitudinal velocity fluctuations (process I) through the energy production term $\{-\overline{uv}\partial\overline{U}/\partial y\}$ in the near-wall region (Figure 11). Then, some energy from the longitudinal velocity fluctuations transfers to the cross-stream velocity fluctuations at a higher wave number range (Figures 12 and 13) through the return-to-isotropy terms, which seem to be the only communication channel between the u'^2 and v'^2 transport equations (process II). The Reynolds shear stress, which is driven by the cross-stream velocity fluctuations as shown in Figure 14, increases, extracting more energy from the mean flow via the production term

$$\left\{-\rho\overline{v'^2}\frac{\partial\overline{U}}{\partial y}\right\}$$

(process III). The increased turbulent shear stress then extracts more energy from the mean flow to u' through process I again. This energy transfer process forms the main routes for production of u', v', and $\overline{uv}$ (processes I, II, and III) with supplying pipelines of energy from the mean flow that have branches to each component through diffusion and dissipation. At the same time, the cascading process transfers the low wave number fluctuation energy to the high wave number fluctuation energy in the wave number domain, and the energy is dissipated into heat. Dissipations of u' and v' reach the "asymptotic spectra" (Figures 19 and 20) of typical turbulent boundary layer profiles first, followed by the v'^2 spectrum (Figures 10, 13, and 17). Once v'^2 attains the asymptotic spectrum, the production of the Reynolds shear stress reaches its limit, and the energy transfer from the mean flow to the longitudinal velocity fluctuations becomes saturated. Eventually, u'^2 starts to decay (Figure 10) because of the limited supply of energy from the mean flow and constant dissipation through the cascading process; it reaches the asymptotic state last. This scenario is based on spectral information obtained from maximum u' locations in the boundary layer and along the streamwise direction. The effect of diffusion across the boundary layer is not included in the above discussion.

Spectral analogy between velocity and temperature fluctuations

Comparisons of the normalized power spectra among the u, v, and t fluctuations at the maximum u' locations for station 6 and station 12 are shown in Figures 21 and 22. As is evident in these figures, the thermal power spectra of the t temperature fluctuations are very close to the spectra of the u velocity fluctuations in the early transitional region with a large portion of energy contained in the wave number range less than 80 m^{-1}. Conversely, the v spectrum contains more energy in the higher wave number range with a maximum value around 500 m^{-1} (Figure 21). In the early turbulent region at station 12, a large portion of the energy of u and t has moved to wave numbers higher than 80 m^{-1} (Figure 22). It is interesting to see all three curves in Figure 22 cross at the same wave number, approximately 180 m^{-1}, which happens to be the most amplified wave number at station 5 in Figure 13. The implication of this synchronized "cross-over"

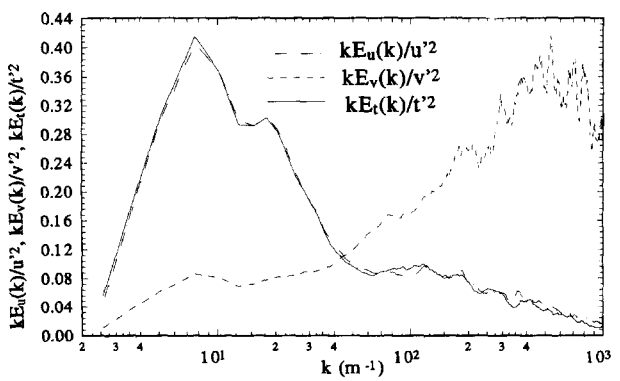

Figure 21 Comparison among $E_u(k)$, $E_v(k)$, and $E_t(k)$ at the maximum u' location of station 6 for the baseline case

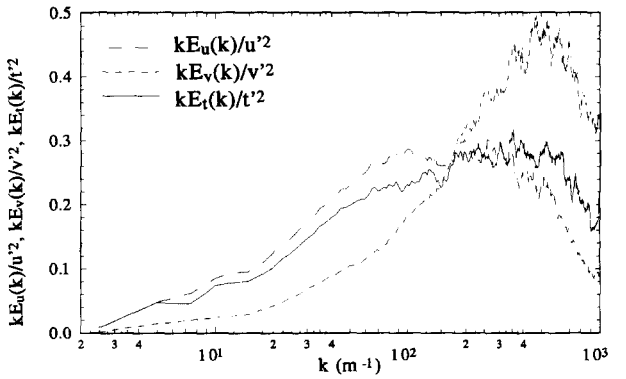

Figure 22 Comparison among $E_u(k)$, $E_v(k)$, and $E_t(k)$ at the maximum u' location of station 12 for the baseline case

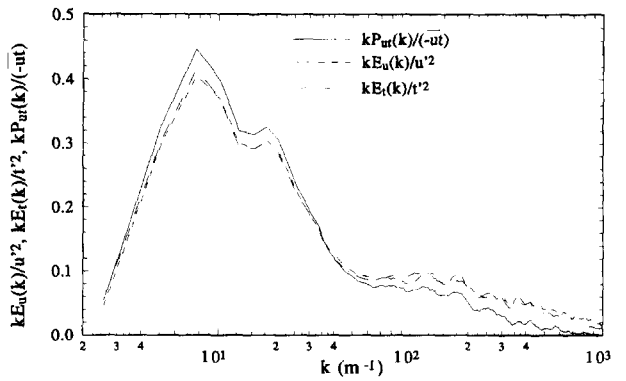

Figure 23 Comparison among $E_u(k)$, $E_t(k)$, and $P_{ut}(k)$ at the maximum u' location of station 6 for the baseline case

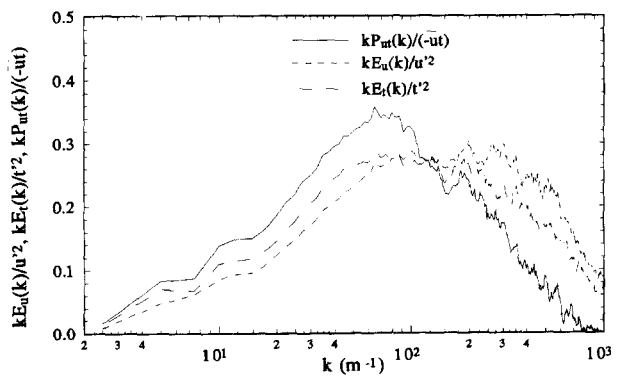

Figure 24 Comparison among $E_u(k)$, $E_t(k)$, and $P_{ut}(k)$ at the maximum u' location of station 12 for the baseline case

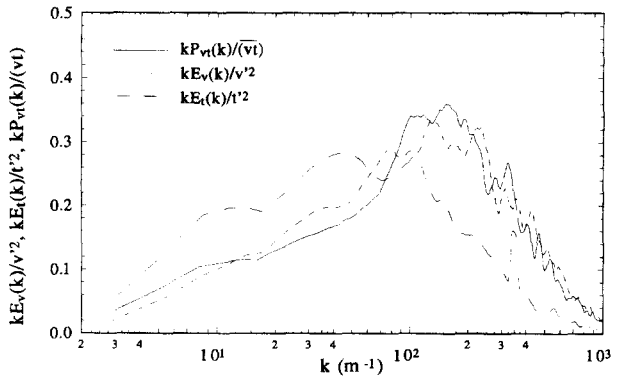

Figure 25 Comparison among $E_v(k)$, $E_t(k)$, and $P_{vt}(k)$ at the maximum u' location of station 6 for the baseline case

can be interpreted as the impact of the v fluctuations on the t fluctuations. If we look back at the spectra in the transitional region in Figure 21, u and t almost exactly overlapped; however, in the early turbulent region in Figure 22, the t curve seems to be pulled down by the v curve in the wave number range less than 180 m^{-1} and pulled up by the v curve above 180 m^{-1}. Although the deviation of t from u is not large, the effect of v on passive temperature fluctuations is very significant, because the magnitude of the v fluctuations is smaller than that of the u fluctuations. It should be noted that the magnitudes in Figure 22 are normalized values.

Comparison among the normalized spectra of the u and t fluctuations and their cospectra for the baseline case is shown in Figure 23 at station 6 and in Figure 24 at station 12. Generally, the correlation between the longitudinal velocity and the temperature fluctuations is better at the low wave number range than at the high wave number range in both the transitional and the turbulent regions. It should be remembered that at wave numbers lower than 120 m^{-1}, the velocity fluctuations are more associated with unsteadiness than with turbulence.

In an elevated FSTI case (6.4%), comparisons among the spectra of v and t fluctuations and their co-spectra in the transition region (station 6) are shown in Figure 25. Similar to the co-spectra between the u and v velocity fluctuations, the co-spectra between the v and t fluctuations are strongly affected by the v spectrum. The $\overline{vt}$ correlation (Figure 25) is better than the $\overline{ut}$ correlation (Figure 23) in the higher wave number range. This may suggest that the cross-stream Reynolds heat flux ($\overline{ut}$) is transported by smaller eddies than is the streamwise Reynolds heat flux ($\overline{vt}$).

Conclusion

A spectral analysis of boundary-layer transition on a heated flat plate was conducted at FSTI = 0.5% and 6.4%. The spectra of u, v, and t and their co-spectra ut and vt were processed at the maximum u' locations of each streamwise measuring station. The linear T–S instability wave amplification was observed in the case with 0.5% FSTI.

The results indicate that the peak location of the turbulence production ($y/\delta \approx 0.1$) coincides with the peak location at u'; whereas, the region of high turbulent shear ($y/\delta \approx 0.35$ or $Y^+ \approx 70$) produces little turbulence energy. The high turbulent shear stress was speculated to be associated with the break-up activity of the hairpin vortices.

Once the transition starts, a large fraction of u' energy is contained in the lower wave number range (less than 60 m^{-1}); whereas, the v'^2 energy is contained in the higher wave number range (near 600 m^{-1} and beyond). A primary energy transfer process for a transitional boundary layer is hypothesized (Figure 18). The return to isotropy terms play an important role in transferring u component energy to the v component, especially in the high wave number range. The v spectrum reaches the asymptotic distribution of a typical turbulent boundary layer faster than the u spectrum does during the streamwise evolution in the transitional region (Figures 10, 12, and 13). The turbulent shear stress (uv) was predominantly driven by v even in the presence of higher magnitudes of u. The dissipation power spectra for both u and v evolves faster than the turbulence power spectra of u and v in the transitional process.

The power spectrum of the temperature fluctuations coincides with that of the longitudinal velocity fluctuations in the early to middle transitional flow, but it is significantly affected by the v spectrum in the late transitional and early turbulent flow regions. The correlation between the u velocity fluctuations and the temperature fluctuations is stronger at a low wave number range than at a high wave number range. For the elevated free-stream turbulence intensity case, the turbulence energy is contained in a narrower wave number band than in the low turbulence intensity case. The cross-stream Reynolds heat flux ($\overline{vt}$) is transported by smaller eddies than is the streamwise Reynolds heat flux ($\overline{ut}$).

References

Blair, M. F. 1992. Boundary layer transition in accelerating flows with intense free-stream turbulence, Part 1 — Disturbances upstream of transition onset; Part 2 — The zone of intermittent turbulence. *J. Fluids Eng.* **114**, 313–332

Chua, L. P. and Antonia, R. A. 1990. Turbulent Prandtl number in a circular jet. *Int. J. Heat Mass Transfer*, **33**, 331–339

Emmons, H. W. 1951. The laminar-turbulent transition in a boundary layer — Part I. *J. Aeronaut. Sci.* **18**, 490–498

Keller, F. J. 1993. Flow and thermal structures in heated transitional boundary layers with and without streamwise acceleration. Ph.D. dissertation, Department of Mechanical Engineering, Clemson University, Clemson, SC, USA

Kim, J., Simon, T. W. and Kestoras, M. 1994. Fluid mechanics and heat transfer measurements in transitional boundary layers conditionally sampled on intermittency. *J. Turbomachinery*, **116**, 405–416

Kuan, C. L. 1987. An experimental investigation of intermittent behavior in the transitional boundary layer. M.S. thesis, Department of Mechanical Engineering, Clemson University, Clemson, SC, U.S.A.

Kuan, C. L. and Wang, T. 1989. Some intermittent behavior of transitional boundary layers. AIAA Paper 89-1890

Kuan, C. L. and Wang, T. 1990. Investigation of intermittent behavior of transitional boundary layers using a conditional averaging technique. *Exp. Thermal Fluid Sci.* **3**, 157–170

Narasimha, R. 1958. On the distribution of intermittency in the transition region of a boundary layer. *J. Aeronaut. Sci.* **24**, 711–712

Shome, B. 1991. Development of a three-wire probe for the measurement of Reynolds stresses and heat fluxes in transitional boundary layers. M.S. thesis, Department of Mechanical Engineering, Clemson University, Clemson, SC, USA

Sohn, K. H. and Reshotko, E. 1991. Experimental study of boundary layer transition with elevated free-stream turbulence on a heated flat plate. NASA CR-187068

Suder, K. L., O'Brien, J. E. and Reshotko, E. 1988. Experimental study of bypass transition in a boundary layer transition. NASA TM-100913

Wang, T., Keller, F. J. and Zhou, D. 1992. Experimental investigation of Reynolds shear stresses and heat fluxes in a transitional boundary layer. In *Fundamental and Applied Heat Transfer Research for Gas Turbine Engines*, ASME HTD — Vol. 226, 61–70

Wang, T., Keller, F. J. and Zhou, D. 1996. Flow and thermal structures in a transitional boundary layer. *Exper. Thermal Fluid Sci.*, to appear

Zhou, D. 1993. Effects of elevated free-stream turbulence and streamwise acceleration on flow and thermal structures in transitional boundary layers. Ph.D. Dissertation, Department of Mechanical Engineering, Clemson University, Clemson, SC, U.S.A.

Zhou, D. and Wang, T. 1995. Effects of elevated free-stream turbulence on flow and thermal structures in transitional boundary layers. *J. Turbomachinery*, **117**, 407–417